MAJOR ARTICLE

Plasma Metabolomic Profiling of Patients Recovered From Coronavirus Disease 2019 (COVID-19) With Pulmonary Sequelae 3 Months After Discharge

Juanjuan Xu,[1,a] **Mei Zhou,**[1,a] **Ping Luo,**[2,a] **Zhengrong Yin,**[1,a] **Sufei Wang,**[1,a] **Tingting Liao,**[1,a] **Fan Yang,**[3] **Zhen Wang,**[1] **Dan Yang,**[1] **Yi Peng,**[1] **Wei Geng,**[1] **Yunyun Li,**[1] **Hui Zhang,**[1] **and Yang Jin**[1]

[1]Department of Respiratory and Critical Care Medicine, NHC Key Laboratory of Pulmonary Diseases, Union Hospital, Tongji Medical College, Huazhong University of Science and Technology, Wuhan, Hubei, China; [2]Department of Translational Medicine Center, Union Hospital, Tongji Medical College, Huazhong University of Science and Technology, Wuhan, Hubei, China; and [3]Department of Radiology, Union Hospital, Tongji Medical College, Huazhong University of Science and Technology, Wuhan, Hubei, China

Background. Elucidation of the molecular mechanisms involved in the pathogenesis of coronavirus disease 2019 (COVID-19) may help to discover therapeutic targets.

Methods. To determine the metabolomic profile of circulating plasma from COVID-19 survivors with pulmonary sequelae 3 months after discharge, a random, outcome-stratified case-control sample was analyzed. We enrolled 103 recovered COVID-19 patients as well as 27 healthy donors, and performed pulmonary function tests, computerized tomography (CT) scans, laboratory examinations, and liquid chromatography-mass spectrometry.

Results. Plasma metabolite profiles of COVID-19 survivors with abnormal pulmonary function were different from those of healthy donors or subjects with normal pulmonary function. These alterations were associated with disease severity and mainly involved amino acid and glycerophospholipid metabolic pathways. Furthermore, increased levels of triacylglycerols, phosphatidylcholines, prostaglandin E2, arginine, and decreased levels of betain and adenosine were associated with pulmonary CO diffusing capacity and total lung capacity. The global plasma metabolomic profile differed between subjects with abnormal and normal pulmonary function.

Conclusions. Further metabolite-based analysis may help to identify the mechanisms underlying pulmonary dysfunction in COVID-19 survivors, and provide potential therapeutic targets in the future.

Keywords. COVID-19; metabolomics; lipidomics; pulmonary function.

Severe acute respiratory syndrome coronavirus 2 (SARS-CoV-2) is a highly pathogenic respiratory virus with high infection and fatality rates. Previous studies have shown that, despite recovery from severe acute respiratory syndrome (SARS), survivors had unresolved health issues, such as persistence of active alveolitis and impairment of gas diffusion [1, 2]. Early analysis of coronavirus disease (COVID-19) survivors suggests a high rate of lung function abnormalities [3–6].

Treatment options for pulmonary fibrosis are limited [7]. Therefore, there is a critical need to identify the molecular pathways involved in the development of pulmonary fibrosis and

to develop novel treatment strategies. Metabolomics, a rapidly emerging field of "omics" research, can provide pathobiological molecular profiles that encompass both microbial and host interactions. This makes it a valuable tool for identification of biomarkers associated with disease development pathways, and for understanding the biological mechanisms driving the pathogenetic pathways.

Metabolomics approaches were useful for identifying novel biomarkers and new pathobiological pathways associated with viral infections. SARS-CoV-2 infection has been demonstrated to cause multiple organ failure, suggesting systemic pathological effects [8]. Such systemic alterations may be reflected by a change in the levels of plasma metabolites. Therefore, we used plasma samples from COVID-19 survivors to profile their plasma metabolomes.

METHODS

Study Design and Participants

A total of 130 participants were ultimately included in this prospective study, including 34 mild/moderate patients (RMs), 69 severe/critical patients (RCs) who had been discharged from Wuhan Union Hospital for 3 months, and 27 uninfected healthy donors (HDs) who were matched for sex and body mass index

(BMI) as controls. We excluded participants with the underlying lung diseases. All participants were negative for the SARS-CoV-2 nucleic acid, as confirmed by real-time polymerase chain reaction testing upon recruitment. The patients recovered from COVID-19 (recovered patients: RPs) were diagnosed and stratified at admission according to the New Coronavirus Pneumonia Prevention and Control Program (7th Edition) released by the National Health Commission of China (see details in Supplementary Table 1).

We collected case information and contact information of COVID-19 RPs who were discharged between March 1 and March 30, 2020 in Wuhan Union Hospital, against mandatory discharge criteria (normal body temperature lasting longer than 3 days; respiratory symptoms improved significantly; negative results of 2 consecutive SARS-CoV-2 RNA tests at least 24 hours apart). RPs who met the inclusion criteria and were willing to participate were interviewed face-to-face in the outpatient clinic of Wuhan Union Hospital at the point of 3 months after discharge. At the visit, each participant received the nucleic acid test and antibody detection for SARS-COV-2, pulmonary-function test, and chest computed tomography (CT) scan. Routine blood test, biochemical and coagulation tests were completed at the same time. Their peripheral blood samples were stored at -80 ℃ for subsequent metabolite detection.

Chest CT Scanning, Artificial Intelligence-Based Quantitative Analysis of CT Images, and Pulmonary Function Test
The standard protocol used here is in accordance with previously published method [9–11], and details are listed in Supplementary Methods.

Metabolomic Profiling
A liquid chromatography-electrospray ionization-tandem mass spectrometry (LC-ESI-MS/MS) system (Shim-pack UFLC SHIMADZU CBM A UPLC system, coupled with QTRAP® 6500 + System MS) was used to analyze metabolites. To detect metabolites as much as possible, the hydrophilic and hydrophobic metabolites were respectively extracted and analyzed as per previously reported methods [12], and details have been listed in Supplementary Methods. The list of multiple reaction monitoring (MRM) transitions of detected metabolite is shown in Supplementary Table 2. Peak areas of metabolites and lipids were obtained using the Analyst software (version 1.6.3).

Statistics
Orthogonal partial least square-discriminate analysis (OPLS-DA) was conducted using SIMCA-P software (version 11.0; Umetrics). For clinical characteristics, laboratory tests, and artificial intelligence of chest CT data analyses, Kruskal-Wallis (K-W) test for multiple groups and Mann-Whitney U test for 2 groups were used for continuous variables, and chi-square test or Fisher's exact test for category variables. For lung function comparison between the 3 groups, analysis of covariance was used for continuous variables by setting the age and comorbidities as the covariates, chi-square test or Fisher's exact test for all category variables. For metabolite profile comparison between every 2 groups, the metabolite profiles were first log transformed, then linear regression models were fitted for each metabolite profile by setting the age and comorbidities as covariates. In addition, for metabolite profile multiple tests, we used the false discovery rate (FDR) to control the false positive (FDR < 0.1 and P value < .05). The Spearman correlations among the differential metabolites and clinical indices were calculated for correlation analyses. The statistical analyses were conducted by SPSS software (version 18.0.0) and R software (version 3.6.3). Heatmaps of differential metabolites and relationships were displayed using the Multi Experiment Viewer software (MeV, version 4.7.4). Analyses of metabolite enrichment were conducted using the Metaboanalyst online software (http://www.metaboanalyst.ca/).

RESULTS

Demographic and Clinical Features of Recovered COVID-19 Patients
Each of the 103 recovered COVID-19 patient was enrolled at 3 months after their discharge. Twenty-seven HDs were included at the same time. Compared with RPs, HDs had significantly less comorbidity, and the only comorbidity in any of the HDs was hypertension. Moreover, all the included HDs were confirmed as having almost normal CT scans and normal pulmonary function tests (PFTs). More than 80% RPs tested IgG positive for SARS-Cov2 (Table 1), suggesting the importance of humoral immunity in their recovery. In RMs or RCs, factors indicative of poor prognosis, namely lymphopenia and increased aspartate transaminase levels, had returned to normal levels compared with those of HDs. However, laboratory parameters related to liver function (total bilirubin [TBIL], direct bilirubin [DBIL], albumin/globulin [A/G]) and renal function (Cys-C) remained aberrant in RMs or RCs, compared with those in HDs.

Analysis of CT Images in COVID-19 Survivors
Furthermore, 22 HDs and 98 RPs (32 RMs and 66 RCs) underwent chest CT, which revealed the presence of lung lesions in patients in the recovered groups (Table 2). Artificial intelligence (AI)-derived CT features for quantifying pneumonia lesions were studied to assess lung rehabilitation. All the findings indicated that the impact of COVID-19 on lungs persisted in RMs and RCs. More lesion involvement appeared in the right lung lower lobe of RCs compared to the RMs. Moreover, ground-glass opacities (GGO), the most common radiological abnormality identifiable at admission, was of significantly higher

Table 1.   Clinical Characteristics and Laboratory Tests of Recovered COVID-19 Patients Grouped by Illness

Characteristics	Group (N = 130)			P value
	Healthy donors (n = 27)	RMs (n = 34)	RCs (n = 69)	
Age, median (IQR), years	49.00 (38.00–57.00)	56.00 (44.75–63.25)	61.00 (55.00–68.00)	<.0001
Sex				
Female, n (%)	14 (51.9%)	20 (58.8%)	37 (53.6%)	.84
BMI, median (IQR), kg/m^2	23.39 (20.55–25.29)	24.01 (22.49–25.53)	24.35 (22.46–26.64)	.16
Serum antibody (n = 127 / 130)				
IgM Positive, n (%)	0 (0.0%)	3 (8.8%)	8 (12.1%)	.18
IgG Positive, n (%)	1 (3.7%)	29 (85.3%)	64 (97.0%)	<.0001
Comorbidities	3 (11.1%)	20 (60.6%)	44 (64.7%)	<.0001
Hypertension	3 (11.1%)	8 (24.2%)	29 (42.6%)	.0069
Hyperlipidemia	0 (0.0%)	8 (24.2%)	13 (19.1%)	.012
Diabetes	0 (0.0%)	5 (15.2%)	16 (23.5%)	.0096
Heart disease	0 (0.0%)	2 (6.1%)	7 (10.3%)	.27
Cerebrovascular disease	0 (0.0%)	0 (0.0%)	1 (1.5%)	1.00
Liver disease	0 (0.0%)	2 (6.1%)	7 (10.3%)	.27
Kidney disease	0 (0.0%)	0 (0.0%)	1 (1.5%)	1.00
Solid tumor	0 (0.0%)	2 (6.1%)	2 (2.9%)	.53
LDH, U/L	190.00 (181.00–228.00)	205.00 (185.00–240.50)	233.50 (201.50–267.00)	.0052
CRP, median (IQR), mg/L	0.39 (0.11–1.09)	0.73 (0.16–1.45)	1.25 (0.49–2.32)	.0032
Hemotologic indicators, median (IQR)				
WBCs, x10^9/L	4.98 (4.37–6.42)	5.27 (4.35–6.67)	5.45 (4.34–6.20)	.95
Neutrophil count, x10^9/L	3.46 (2.340–4.205)	3.05 (2.56–3.95)	3.14 (2.41–4.02)	.96
Lymphocyte count, x10^9/L	1.74 (1.38–2.00)	1.61 (1.42–2.04)	1.65 (1.35–2.03)	.80
Neutrophil-to-lymphocyte ratio	1.90 (1.64–2.61)	1.81 (1.47–2.32)	1.86 (1.45–2.59)	.73
Liver function indicators, median (IQR)				
TBIL, μmol/L	16.90 (13.70–20.25)	14.10 (10.75–19.55)	13.70 (11.00–16.90)	.024
DBIL, μmol/L	5.80 (4.85–6.70)	5.15 (3.58–6.73)	5.10 (3.80–6.00)	.053
ALT, U/L	18.00 (13.00–25.50)	18.00 (13.25–26.75)	22.00 (14.00–28.00)	.66
AST, U/L	22.00 (19.50–24.00)	19.50 (17.00–24.75)	21.00 (19.00–26.00)	.39
ALP, U/L	70.00 (65.00–85.50)	76.50 (67.00–87.00)	77.00 (62.00–95.00)	.70
GGT, U/L	19.00 (13.00–41.00)	20.00 (17.25–26.00)	22.00 (18.00–29.00)	.52
TP, g/L	76.50 (73.75–79.50)	75.95 (74.18–80.18)	77.00 (74.90–78.80)	.92
Albumin, g/L	47.50 (45.85–48.65)	47.15 (45.33–48.10)	45.60 (44.10–47.40)	.0077
Globin, g/L	29.00 (27.85–31.20)	29.70 (26.75–33.03)	31.30 (29.00–33.40)	.11
A/G	1.60 (1.50–1.70)	1.50 (1.50–1.70)	1.50 (1.40–1.60)	.022
Renal function indicators, median (IQR)				
Creatinine, μmol/L	68.60 (63.70–77.05)	68.60 (62.40–75.90)	71.65 (63.93–77.88)	.65
BUN, mmol/L	5.20 (4.30–5.85)	5.00 (4.625–5.93)	5.10 (4.43–5.98)	.96
Cys-C, mg/L	0.95 (0.87–1.10)	0.99 (0.87–1.15)	1.06 (0.96–1.32)	.017
Coagulation function indicators, median (IQR)				
PLT, x10^9/L	209.00 (157.50–262.50)	212.50 (184.00–236.00)	211.00 (169.00–245.00)	.93
D-Dimer, μg/mL	0.29 (0.25–0.37)	0.36 (0.29–0.45)	0.41 (0.29–0.54)	.0043
PT, s	12.90 (12.60–13.30)	13.10 (12.70–13.60)	12.80 (12.40–13.40)	.34
APTT, s	35.80 (34.10–39.25)	36.30 (33.70–37.20)	36.40 (33.70–38.40)	.86
FIB, g/L	2.90 (2.54–3.38)	3.06 (2.76–3.41)	3.15 (2.90–3.53)	.16
TT, s	16.30 (15.80–16.75)	16.60 (16.20–17.20)	16.50 (16.30–17.50)	.13

Data were presented as median (interquartile range) for continuous variables and n (%) for category variables. Kruskal-Wallis (K-W) test was used for continuous variables and chi-square test or Fisher's exact test for all category variables.

Abbreviations: A/G, albumin/globin; ALP, alkaline phosphatase; ALT, alanine aminotransferase; APTT, activated partial thromboplastin time; AST, aspartate amino transferase; BMI, body mass index; BUN, blood urea nitrogen; CRP, C-reactive protein; Cys-C, cystain C; DBIL, direct bilirubin; FIB, fibrinogen; GGT, γ-glutamyl transpeptidase; IQR, interquartile range; LDH, lactate dehydrogenase; PLT, platelet; PT, prothrombin time; RCs, recovered severe/critical patients; RMs, recovered mild/moderate patients; TBIL, total bilirubin; TP, total protein; TT, thrombin time; WBCs, white blood cells.

ratio in RCs than in RMs. Additional radiological features, such as solid components, appeared more frequently in RCs than in RMs. Overall, there was more right lung involvement in the RCs compared to the RMs.

Pulmonary Dysfunction: One of the Most Common Sequelae in COVID-19 Survivors 3 Months After Discharge

Anomalies were mainly noted in lung volume and diffusion capacity (Table 3), as revealed by significantly reduced total

Table 2. Artificial Intelligence of Chest CT in Recovering COVID-19 Patients Grouped by Illness

Characteristics	Group (N = 120/130)			P value	
	Healthy donors (n = 22)	RMs (n = 32)	RCs (n = 66)	Overall	RMs vs RCs
Age, median (IQR), years	50.00 (39.50–57.00)	56.00 (47.75–63.25)	61.00 (55.00–68.00)	.0002	.012
Sex					
Female, n (%)	12 (54.5%)	19 (59.4%)	36 (54.5%)	.89	-
Pneumonia score calculated by AI, median (IQR)					
Total score	0.00 (0.00–0.00)	2.00 (0.00–4.00)	4.00 (0.00–8.00)	<.0001	.015
Left lung score	0.00 (0.00–0.00)	0.00 (0.00–2.00)	2.00 (0.00–4.00)	<.0001	.026
Right lung score	0.00 (0.00–0.00)	1.00 (0.00–2.00)	2.00 (0.00–6.00)	<.0001	.015
Left lung upper lobe score	0.00 (0.00–0.00)	0.00 (0.00–0.00)	0.00 (0.00–2.00)	.0001	.02
Left lung lower lobe score	0.00 (0.00–0.00)	0.00 (0.00–2.00)	1.00 (0.00–2.00)	.0006	.105
Right lung upper lobe score	0.00 (0.00–0.00)	0.00 (0.00–2.00)	0.00 (0.00–2.00)	.0002	.092
Right lung middle lobe score	0.00 (0.00–0.00)	0.00 (0.00–0.00)	0.00 (0.00–2.00)	.0043	.056
Right lung lower lobe score	0.00 (0.00–0.00)	0.00 (0.00–2.00)	2.00 (0.00–2.00)	<.0001	.025
Lesion ratio of GGO in lungs, median (IQR), %					
Total GGO ratio	0.01 (0.00–0.01)	0.05 (0.010–0.170)	0.42 (0.023–1.51)	<.0001	.012
Left lung GGO ratio	0.01 (0.00–0.028)	0.015 (0.00–0.16)	0.24 (0.01–1.015)	.0001	.011
Right lung GGO ratio	0.00 (0.00–0.00)	0.05 (0.00–0.25)	0.44 (0.02–2.202)	<.0001	.005
Left lung upper lobe GGO ratio	0.00 (0.00–0.018)	0.00 (0.00–0.028)	0.08 (0.00–0.62)	.0003	.004
Left lung lower lobe GGO ratio	0.00 (0.00–0.043)	0.025 (0.00–0.29)	0.105 (0.00–1.14)	.0058	.077
Right lung upper lobe GGO ratio	0.00 (0.00–0.00)	0.00 (0.00–0.15)	0.065 (0.00–1.12)	<.0001	.015
Right lung middle lobe GGO ratio	0.00 (0.00–0.00)	0.00 (0.00–0.00)	0.00 (0.00–0.16)	.0016	.015
Right lung lower lobe GGO ratio	0.00 (0.00–0.0075)	0.025 (0.00–0.19)	0.36 (0.00–2.71)	<.0001	.01
Lesion ratio of solid components in lungs, median (IQR), %					
Total solid components ratio	0.00 (0.00–0.0075)	0.00 (0.00–0.02)	0.01 (0.00–0.05)	.0026	.08
Left lung solid components ratio	0.00 (0.00–0.01)	0.00 (0.00–0.013)	0.01 (0.00–0.03)	.022	.076
Right lung solid components ratio	0.00 (0.00–0.00)	0.00 (0.00–0.03)	0.01 (0.00–0.06)	.0006	.07
Left lung upper lobe solid components ratio	0.00 (0.00–0.01)	0.00 (0.00–0.01)	0.00 (0.00–0.018)	.59	-
Left lung lower lobe solid components ratio	0.00 (0.00–0.00)	0.00 (0.00–0.01)	0.005 (0.00–0.03)	.0027	.066
Right lung upper lobe solid components ratio	0.00 (0.00–0.00)	0.00 (0.00–0.02)	0.005 (0.00–0.02)	.0062	.102
Right lung middle lobe solid components ratio	0.00 (0.00–0.00)	0.00 (0.00–0.00)	0.00 (0.00–0.00)	.013	.048
Right lung lower lobe solid components ratio	0.00 (0.00–0.00)	0.00 (0.00–0.02)	0.015 (0.00–0.128)	.0016	.038
Total lesion ratio in lungs, median (IQR), %					
Total lesion ratio	0.01 (0.00–0.02)	0.05 (0.01–0.22)	0.485 (0.03–1.74)	<.0001	.013
Left lung lesion ratio	0.01 (0.00–0.038)	0.02 (0.00–0.17)	0.24 (0.013–1.04)	.0002	.015
Right lung lesion ratio	0.00 (0.00–0.01)	0.055 (0.00–0.263)	0.49 (0.023–2.30)	<.0001	.006
Left lung upper lobe lesion ratio	0.00 (0.00–0.03)	0.01 (0.00–0.05)	0.08 (0.00–0.623)	.0013	.016
Left lung lower lobe lesion ratio	0.00 (0.00–0.04)	0.03 (0.00–0.30)	0.125 (0.00–1.15)	.0055	.074
Right lung upper lobe lesion ratio	0.00 (0.00–0.00)	0.00 (0.00–0.16)	0.085 (0.00–1.14)	<.0001	.016
Right lung middle lobe lesion ratio	0.00 (0.00–0.00)	0.00 (0.00–0.00)	0.00 (0.00–0.16)	.0024	.027
Right lung lower lobe lesion ratio	0.00 (0.00–0.01)	0.035 (0.00–0.23)	0.40 (0.00–2.88)	<.0001	.015

Data were presented as median (interquartile range) for continuous variables and n (%) for category variables. Kruskal-Wallis (K-W) test was used for continuous variables between 3 groups and chi-square test or Fisher's exact test for all category variables. The comparison of RMs and RCs group was analyzed by Mann-Whitney U test or chi-square test. For variables with overall P values greater than .05, we did not perform subgroup comparisons.
Abbreviations: BMI, body mass index; GGO, ground-glass opacity; IQR, interquartile range; RCs, recovered severe/critical patients; RMs, recovered mild/moderate patients.

lung capacity (TLC), functional residual capacity (FRC), and diffusing capacity of the lungs for CO (DLCO) values in the COVID-19 recovered groups (all $P < .05$).

Global Metabolite Profiles in COVID-19 Survivors vs Uninfected Individuals
A total of 1124 metabolites (Supplementary Table 2) were detected from 127 plasma samples (excluding 3 hemolysis samples). In QC analysis, CV values of more 90% of the metabolites were less than 20%, respectively (Supplementary Figure 1). Fifty-two metabolites were differentially expressed in RMs and RCs, when compared with HDs (Figure 1A). Furthermore,

plasma metabolic alterations in RCs were more significant than that in RMs (Figure 1B, 1C).

Metabolomic Profiling in COVID-19 Survivors With Abnormal Pulmonary Diffusion Capacity
In OPLS-DA analysis, the samples of COVID-19 RPs with normal and abnormal DLCO (ND&RM, ND&RC, AD&RM, and AD&RC) were separated from those of HDs, illustrating their differential plasma metabolite profiles (Figure 2A). Compared with HDs, 51, 37, 95, and 169 metabolites were marked differentials in these 4 groups, respectively (Figure 2B).

Table 3. Pulmonary Function Tests of Recovering COVID-19 Patients Grouped by Illness

Characteristics	Group (N = 121)			P value
	Healthy donors (n = 27)	RMs (n = 32)	RCs (n = 62)	
Age, median (IQR), years	49.00 (38.00–57.00)	56.00 (47.25–63.75)	60.00 (54.75–67.25)	<.0001
Spirometry, median (IQR)				
FEV1 (L), % predicted	99.80 (93.50–111.90)	98.60 (92.85–116.78)	96.65 (89.15–109.38)	.086
<80% pred, n/N (%)	0/27 (0.0%)	2/32 (6.3%)	4/62 (6.5%)	.55
FEV1/FVC, %	78.58 (75.34–82.52)	74.70 (71.54–79.83)	77.27 (73.19–81.24)	.14
<70%, n/N (%)	0/27 (0.0%)	6/32 (18.8%)	10/62 (16.1%)	.038
Lung volume, median (IQR)				
TLC (L) % predicted	98.90 (92.00–105.40)	98.25 (88.23–106.45)	88.80 (81.60–95.58)	.0001
<80% pred, n/N (%)	0/27 (0.0%)	2/32 (6.3%)	13/62 (21.0%)	.007
FRC (L) % predicted	111.30 (104.60–121.90)	102.80 (86.40–122.80)	91.70 (81.25–103.05)	.001
RV (L) % predicted	101.70 (90.70–112.60)	93.55 (86.55–104.65)	83.20 (72.30–92.75)	.0007
<65% pred, n/N (%)	0/27 (0.0%)	0/32 (0.0%)	9/62 (14.5%)	.009
Diffusion capacity, median (IQR)				
DLCO, mmol/min/kPa	8.35 (7.01–8.80)	6.62 (5.88–7.96)	6.22 (5.49–7.29)	.0007
DLCO% predicted	94.30 (86.80–99.60)	83.60 (75.40–93.68)	80.15 (72.90–90.48)	.0002
<80% pred, n/N (%)	0/27 (0.0%)	13/32 (40.6%)	29/62 (46.8%)	<.0001
60%–80% pred, n/N (%)	0/27 (0.0%)	13/32 (40.6%)	26/62 (41.9%)	<.0001
40%–60% pred, n/N (%)	0/27 (0.0%)	0/32 (0.0%)	3/62 (4.8%)	.43
DLCO/VA,mmol/min/kPa/L	1.50 (1.36–1.63)	1.39 (1.22–1.53)	1.41 (1.28–1.56)	.016
DLCO/VA% predicted	94.20 (85.20–103.00)	89.00 (81.53–99.45)	97.15 (84.65–107.15)	.003
<80% pred, n/N (%)	0/27 (0.0%)	7/32 (21.9%)	9/62 (14.5%)	.026
Fractional exhaled nitric oxide, median (IQR)				
FeNO, ppb	17.00 (14.00–24.00)	19.00 (15.00–26.25)	19.00 (15.00–25.00)	.54
CaNO, ppb	5.40 (2.90–7.00)	5.15 (3.43–8.18)	5.60 (3.10–7.90)	.13

Data were presented as median (interquartile range) for continuous variables and n (%) for category variables. Analysis of covariance was used for continuous variables by setting the age and comorbidities as the predictor variables. Chi-square test or Fisher's exact test for all category variables. DLCO was measured through single-breath method.

Abbreviations: BMI, body mass index; CaNO, exhaled alveolar fraction of nitric oxide; DLCO, diffusing capacity of the lung for carbon monoxide; FeNO, fractional exhaled nitric oxide; FEV1, forced expiratory volume in 1 second; FRC, functional residual capacity; FVC, forced vital capacity; IQR, interquartile range; RCs, recovered severe/critical patients; RMs, recovered mild/moderate patients; RV, residual volume; TLC, total lung capacity; VA, alveolar ventilation.

Twenty-one metabolites, including betaine, purine, stearidonic acid, vitamin D3, guanosine, few species of phosphatidylcholines (PCs), were the common differentials in those with abnormal DLCO (Supplementary Table 3).

Additionally, each group exhibited unique metabolite characteristics, such as elevated levels of glycerolipids and decreased levels of some acylcarnitine (AC) and organic acid (OA) in the AD&RC group. Compared with the alterations in the AD&RC group, the difference in the AD&RM group was mild, as evidenced by increased sphingomyelin (SM) and reduced OAs (Figure 2C and 2D).

RPs was clustered according to COVID-19 severity (Figure 2A); this separation was considerably more significant compared
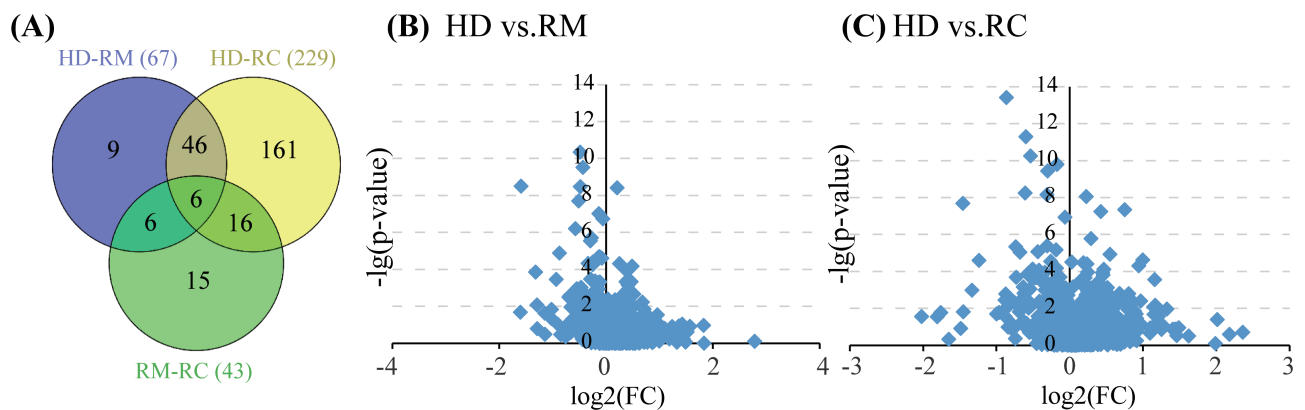
Figure 1. Venn diagram of the number of differential metabolites. (A) Between the comparisons of HD with RM and RC, respectively. (B) and (C) Volcano plots of altered metabolites found in RM and RC compared with HDs, respectively. The X-axis represents the log2 value (FC), FC indicates the ratio of mean level of the metabolite in the RM or RC to the mean value of HDs; the Y-axis denotes the −log(p-value). Abbreviations: HD, healthy donors; RC, severe/critical patients; RM, mild/moderate patients.
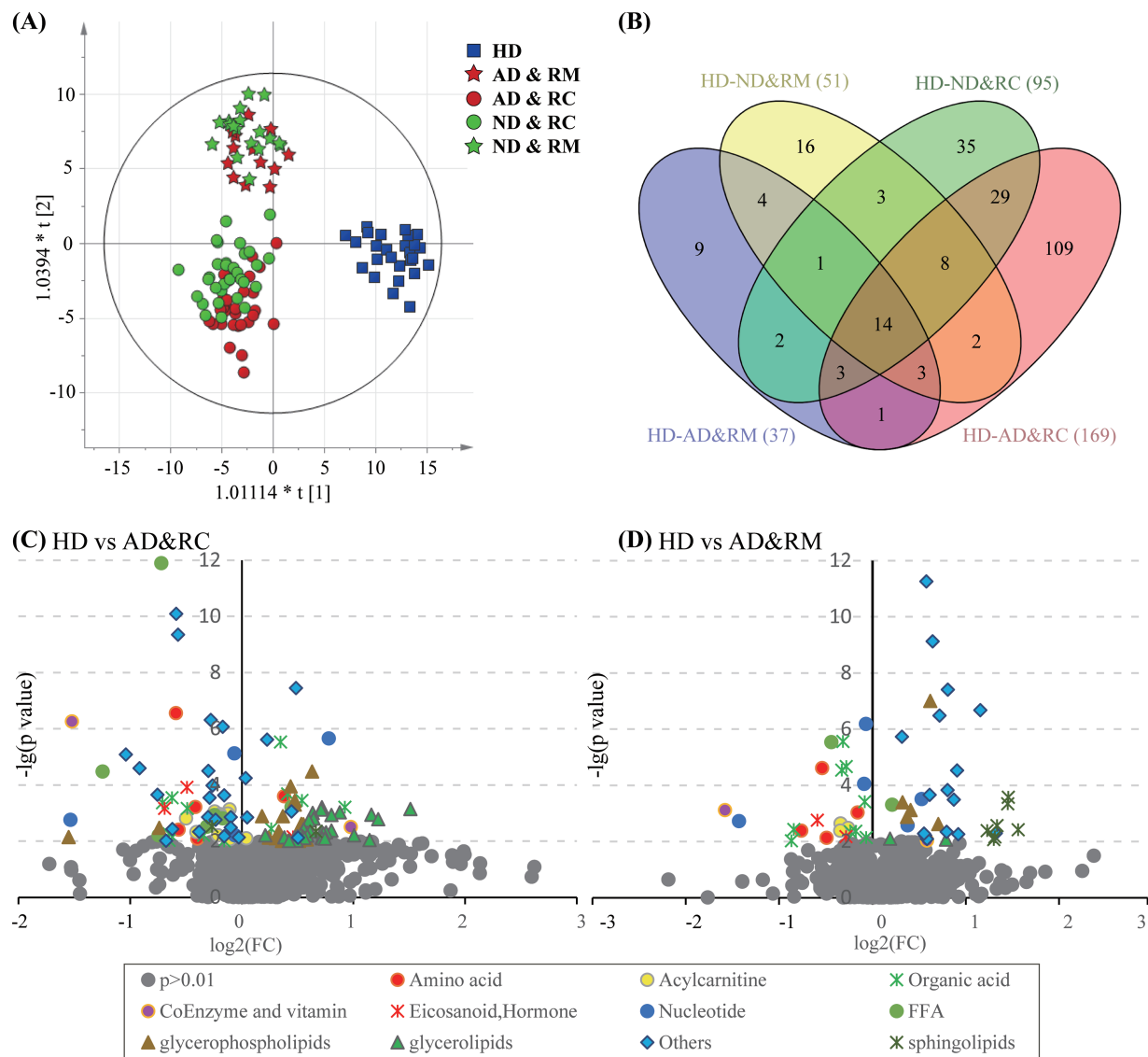
Figure 2. Characterization of metabolic profiles of recovered COVID-19 patients who presented abnormal pulmonary diffusion capacity at 3 months after discharge from the hospital. Recovered (A) score plots of OPLS-DA based on the detected 1124 features (included metabolites and lipids) in the groups of healthy donors, normal or abnormal pulmonary diffusion capacity presented in the recovered mild and severe COVID-19 patients (ND&RM, AD&RM, and ND&RC, AD&RC). (B) Venn diagram displays the number of differential features in the ND&RM, AD&RM, ND&RC, and AD&RC when compared with those in HD. (C) and (D) Volcano plots of altered metabolites found in AD&RC and AD&RM compared with HDs. The X-axis represents the log2(FC) value; FC indicates the ratio of mean level of the metabolite in the AD&RC or AD&RM to the mean value of HDs; the Y-axis denotes −log(p-value). The gray dots represent the metabolites with $P > .01$. Abbreviations: AD&RC, recovered severe/critical patients with abnormal DLCO%pred; AD&RM, recovered mild/moderate patients with abnormal DLCO%pred; COVID-19, coronavirus disease 2019; HD, healthy donors; ND&RC, recovered severe/critical patients with normal DLCO%pred; ND&RM, recovered mild/moderate patients with normal DLCO%pred; OPLS-DA, orthogonal partial least square-discriminate analysis.

to that for DLCO. AD&RM and AD&RC samples presented many unique alterations, such as increased levels of AC, OA, SM in the AD&RM; while increased levels of amino acid (AA), fatty acid (FA), and triacylglycerol (TG) in the AD&RC group (Figure 3A and 3B). Compared with the AD&RM group, decreased short-chain AC, FA, and inversely increased AA and OA were in the AD&RC group (Figure 3C, Supplementary Table 3).

Pathway enrichment of differential metabolites revealed that lysine degradation, taurine and hypotaurine

metabolism, alpha-linolenic acid metabolism, and glycerophospholipid metabolism were mainly disturbed in the subjects with abnormal pulmonary diffusion capacity (Figure 3D and 3E).

Metabolic Characteristics of Patients Recovered From COVID-19 With Abnormal Total Lung Capacity

Thirteen subjects with abnormal DLCO also presented abnormal TLC (AT). Compared with HDs, 111 and 54 metabolites were significantly altered in the normal TLC (NT) and AT
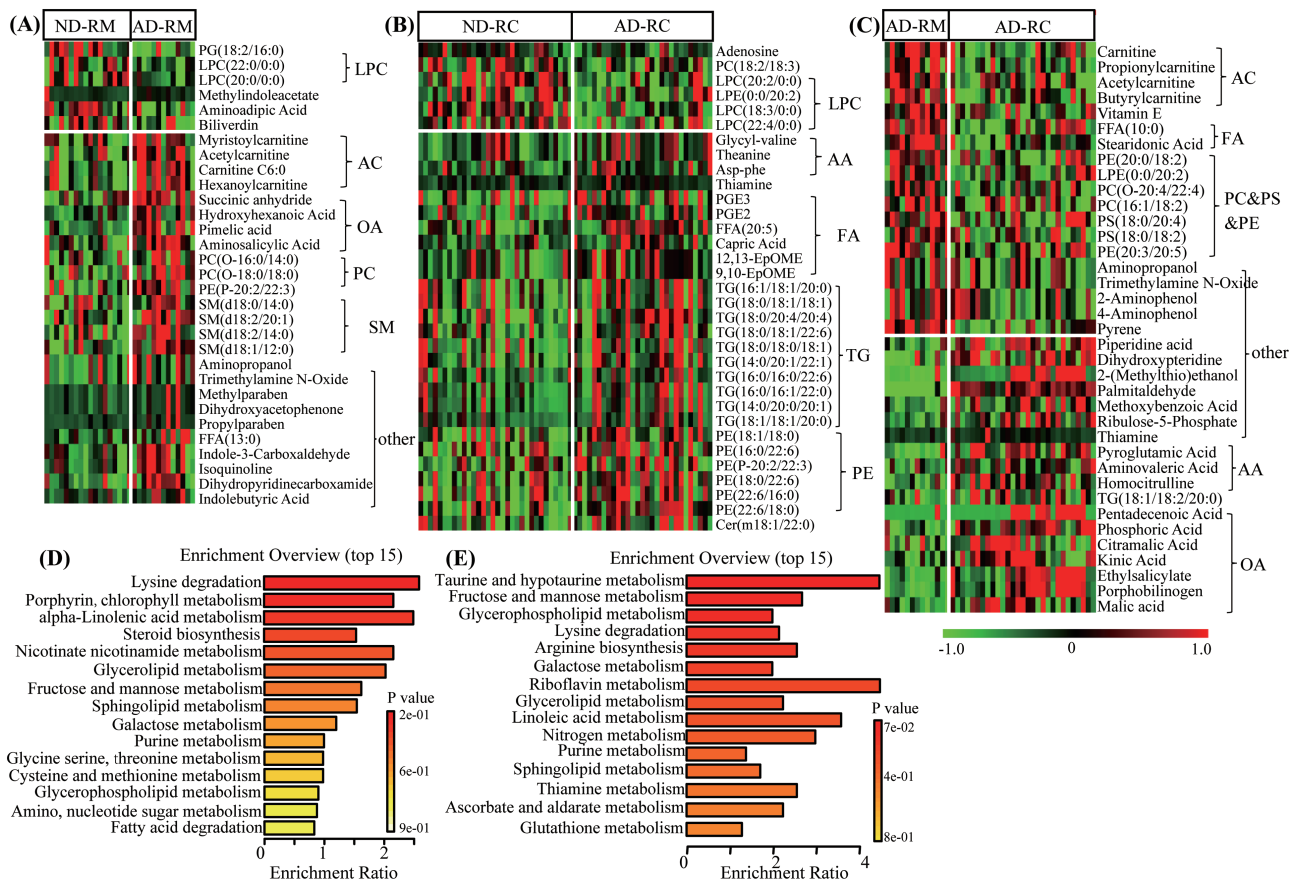
Figure 3. Significantly altered metabolites in COVID-19 survivors presented abnormal pulmonary diffusion capacity at 3 months after their hospital discharge compared to survivors with normal pulmonary diffusion capacity. Heat map of significantly changed lipids and metabolites (*P* < .05 with FC > 1.2 or <0.83) between normal and abnormal pulmonary diffusion capacity survivors of mild (A) or severe (B) type (ND&RM vs. AD&RM, and ND&RC vs. AD&RC), or between recovered mild and severe COVID-19 survivors with abnormal pulmonary diffusion capacity (C) type (AD&RM vs AD&RC) (red, green, and black, denote relative higher, lower and mean level, respectively). (D) (E) Related disturbed pathways of differential metabolites in the AD&RM and AD&RCs, respectively. Abbreviations: COVID-19, coronavirus disease, 2019.

groups, respectively (Figure 4A). Compared with HDs or NT subjects, levels of some FA, such as epoxyeicosatrienoic acid, linolenic acid (FA 18:3), and palmitoleic acid (FA 16:1) were decreased, and acetyltyrosine, acetylleucine, methylhistidine, some species of OA, PC, PE, and AC were increased (Figure 4B). Pathway enrichment analyses of differential metabolites showed that alpha-linolenic acid, arginine, proline, and Vitamin B6 metabolism were mainly disturbed in the AT subjects (Figure 4C).

Metabolite Profiles of COVID-19 Survivors With Abnormal Diffusion Capacity and Chest CT Findings

Thirty and 27 RPs with normal and abnormal DLCO presented abnormal CT findings (ACT&ND and ACT&AD), respectively. Compared with HDs, 44, 73, 63, and 57 metabolites were significantly altered in these 4 groups, respectively (Figure 5A). Compared with abnormal CT groups, levels of OA, methylhisitidine, carnitine C5:1, and TGs were increased in the ACT&AD group, while levels of some TGs and bile acids, including glycocholic acid, glycochenodeoxycholate, and

glycinedeoxycholate were increased in the ACT&ND group (Figure 5B and 5C).

Associations of Differential Metabolites With Clinical Parameters of Pulmonary Functions and CT

During correlation analysis, many differential metabolites displayed significant relationships with the index of pulmonary diffusion capacity. For example, levels of DLCO%pred and DLCO/VA%pred were negatively associated with levels of arginine, and some SM in the RM samples, and levels of prostaglandin E2 (PGE2) and prostaglandin E3 (PGE3), some species of TG in the RC samples (Figure 6A and 6B).

In the association of TLC-related index, many metabolites such as kynurenine, acetyltyrosine, acetylleucine and methylhistidine, some TGs, PCs were negatively correlated with the levels of TLC%pred or RV%pred; conversely, vitamin D3, guanosine, and stearidonic acid were positively associated with this index (Figure 6C).

The levels of total GGO ratio, total solid ratio, or total lesion ratio were negatively correlated with levels of
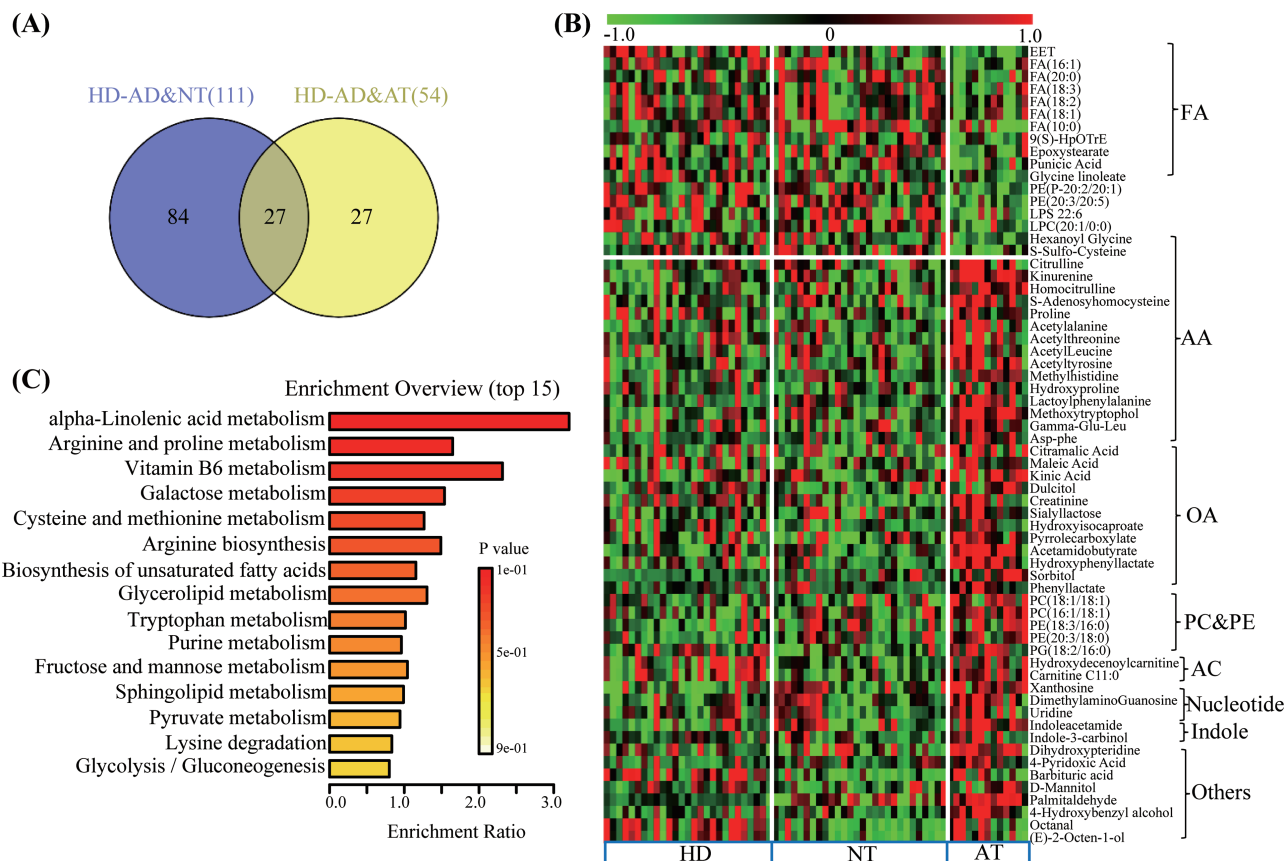
Figure 4. Significantly altered metabolites in COVID-19 survivors who presented abnormal total lung capacity at 3 months after their hospital discharge compared to survivors with normal total lung capacity. (A) Venn diagram showing the number of differential metabolites between the comparisons of HD with NT and AT, respectively. (B) Heat map of differential features (*P* < .05 with FC > 1.2 or <0.83) discovered in the AT group when compared with NT group (red, green, and black denote relatively higher, lower, and mean levels, respectively). (C) Related disturbed pathways of differential lipids and metabolites in the AT group. Abbreviations: AT, abnormal total lung capacity; COVID-19, coronavirus disease 2019; HD, healthy donors; NT, normal total lung capacity.

taurocholic acid, guanosine, trihydroxythrombadienoate, and hydroxymethylacetophenone; conversely, they were positively correlated with levels of citrulline and TG (Figure 6D).

DISCUSSION

Our results demonstrated that the COVID19 survivors who had more severe/critical infection also had more abnormal PFTs. Pathway analysis revealed that these alterations related to abnormal pulmonary function mainly involved the metabolic pathways of arginine biosynthesis, and metabolism of arginine, proline, taurine, hypotaurine, glycerophospholipid, glycerolipid, =and sphingolipid. This may suggest that the metabolic alterations appear to be a marker of more severe clinical presentations, as well as more abnormal PFTs.

Impaired diffusion capacity is the most common lung function abnormality. Among plasma metabolic alterations, we found that lipid alterations in RPs with abnormal diffusion capacity were significant (Figures 2 and 3). Furthermore, these alterations were associated with COVID-19 severity (Figure 3C). Among these lipids, levels of TG and PC were remarkably

associated with the levels of DLCO%pred, or DLCO/VA%pred (Figure 6A and 6B). Previous studies revealed that the levels of TG and PC were significantly altered in COVID-19 patients [12–14], while the high levels of TG (18:2/18:3/20:4) and low levels of PC (18:0/20:3) can be used as potential biomarkers of COVID-19 [12]. Even at 3 months after discharge, levels of many individual TGs remained significantly high in COVID-19 RPs, especially in the RCs. TGs were negatively associated with DLCO% pred. TG is a major energy storage molecule in cells. Excessive accumulation of TG in humans is associated with metabolic diseases and diabetes [15]. Similarly, there is a negative correlation between TG levels and DLCO among hyperlipemic patients, which may be related to alterations in surface-active lipoproteins in the lungs, caused by hyperlipoproteinemia or fat microembolism [16]. Since COVID-19 particularly affects the lungs, we hypothesize that SARS-CoV-2 may reduce DLCO by modulating pulmonary surface-active lipoproteins, thereby causing more TGs to be released into the circulation. This effect may be long-lasting among COVID-19 survivors, even at 3 months after discharge. Therefore, improvement of TG
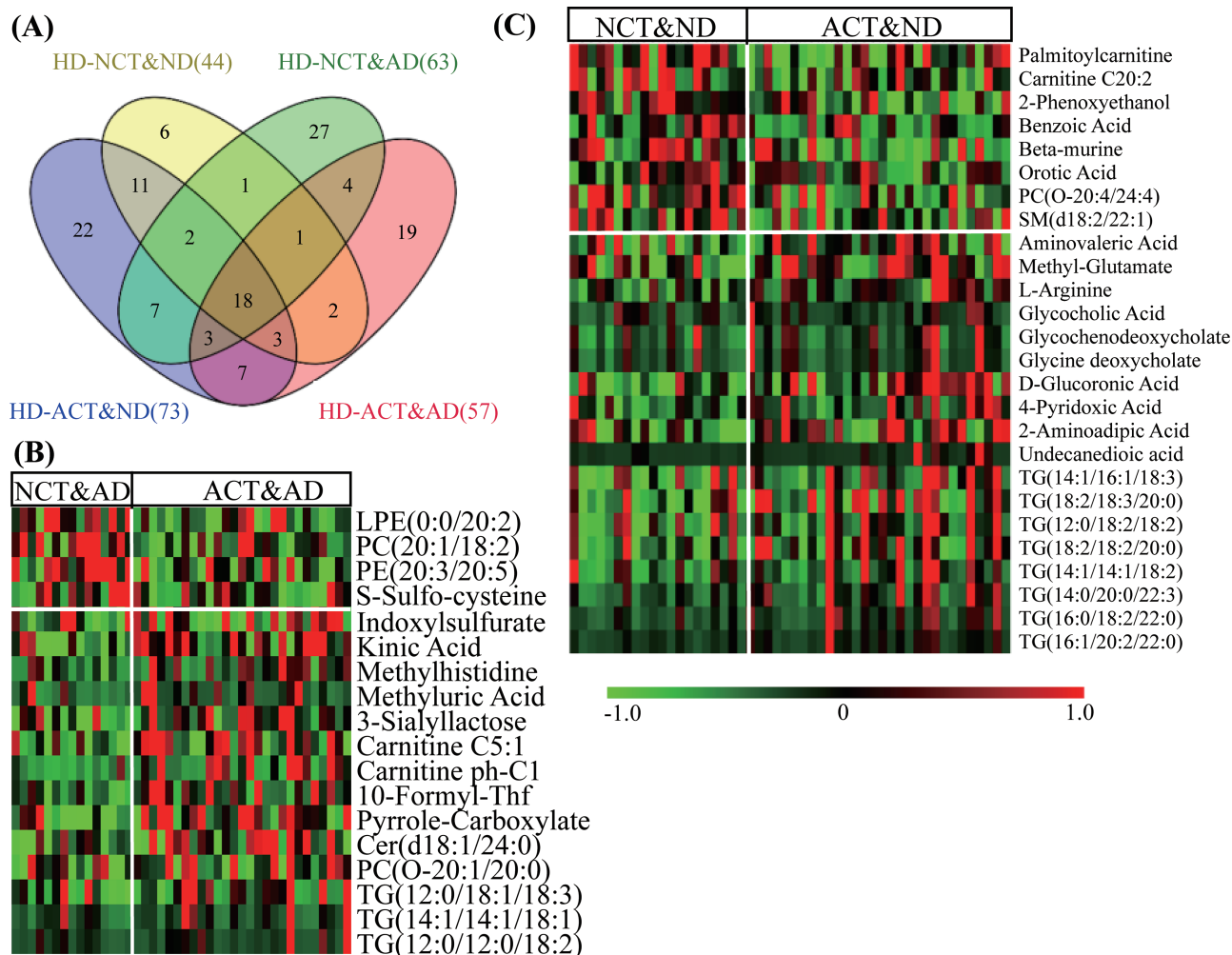
Figure 5. Significantly altered metabolites in COVID-19 survivors who presented abnormal CT results at 3 months after their hospital discharge. (A) Venn diagram showing the number of differential metabolites between the comparisons of HD and ND&NCT, ND&ACT, AD&NCT, and AD&ACT,AT. Heat map of differential features discovered in the ACT groups when compared with NCT groups with abnormal (B) and normal (C) pulmonary diffusion capacity. Red, green, and black denote relatively higher, lower, and mean levels, respectively. Abbreviations: AD&RC, recovered severe/critical patients with abnormal DLCO%pred; AD&RM, recovered mild/moderate patients with abnormal DLCO%pred; HD, healthy donors; ND&RC, recovered severe/critical patients with normal DLCO%pred; ND&RM, recovered mild/moderate patients with normal DLCO%pred.

metabolism may provide a novel strategy for identification of therapeutic targets.

Prostaglandin E2 (PGE2), an eicosanoid, is a major immune mediator, and is used as a therapeutic target for treating various diseases [17]. Additionally, PGE2 is upregulated in cases of influenza A virus (IAV) and Helicobacter infections, which may inhibit the production of type I interferon and cause apoptosis in macrophages to further accelerate viral replication [18, 19]. Additionally, PGE2 inhibition can suppress antigen presentation and T-cell-mediated immunity. Targeted suppression of PGE2 has been shown to improve survival against IAV infection [18]. In our study, PGE2 levels were higher in the AD&RC group than those in ND&RC group. Furthermore, PGE2 levels were negatively associated with DLCO%pred and DLCO/VA%pred values. These trends have also been reported in patients with interstitial pneumonia and chronic obstructive

pulmonary disease (COPD) [20, 21]. PGE2 elevation among abnormal DLCO COVID-19 survivors might indicate their altered inflammation status.

Amino acid metabolism was dramatically altered in the plasma samples of those with abnormal lung function. Arginine plays an important role in regulating T-cell metabolism and in mediating immune response [22]. Arginine concentration is reportedly increased in the lungs of Pseudomonas-infected mouse [23]. Additionally, the expression of arginase or nitric oxide synthase—enzymes necessary for arginine catabolism—are reportedly linked to airway remodeling in COPD [24], smooth muscle relaxation, and vasodilation [25]. Herein, elevated arginine levels may be related to cellular immune status or airway remodeling in COVID-19 RPs with abnormal DLCO.

We also found that betaine levels decreased in the AD&RC group. Betaine is a crucial methyl donor and osmoprotectant. It
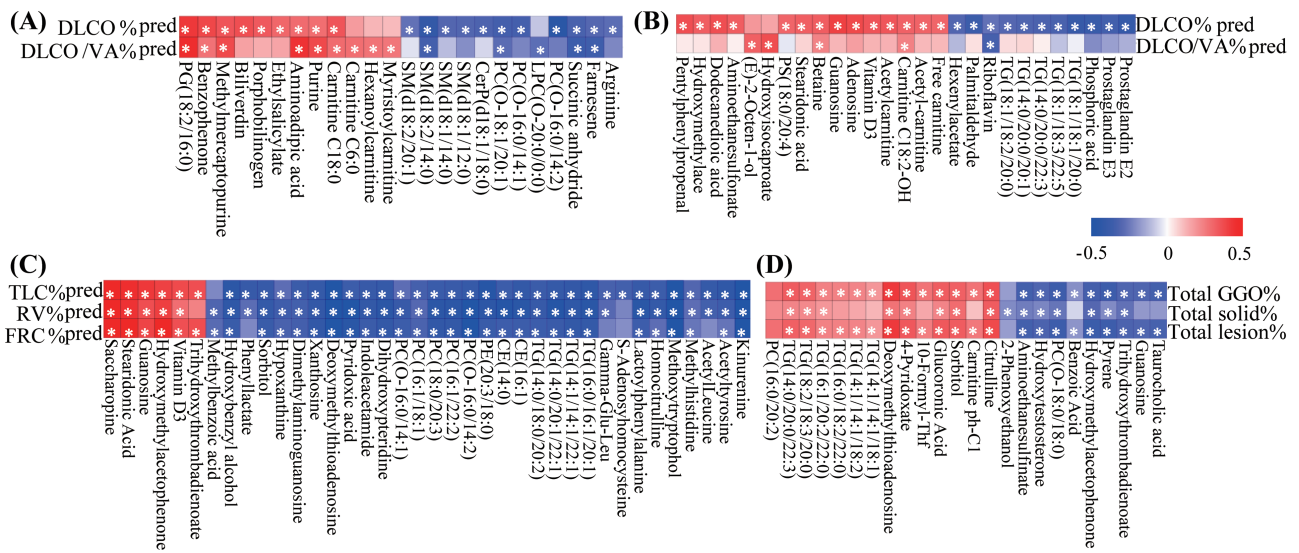
Figure 6. Correlation analysis between clinical parameters and differential metabolites. Heat map of coefficients of Spearman correlation analysis between levels of differential metabolites and pulmonary diffusion capacity parameters in the recovered mild (A) and severe (B) COVID-19 patients. Heat map of coefficients of Spearman correlation analysis between levels of differential metabolites and clinical parameters of abnormal total lung capacity (C) or CT (D). Red, blue, and white denote relatively higher, lower, and mean levels, respectively. Correlations with $P < .05$ are marked with stars(*). Abbreviations: COVID-19, coronavirus disease-2019; CT, computed tomography.

is important for many biological processes, such as resisting oxidative stress by improving the metabolism of sulfur-containing amino acids, by alleviating apoptosis and endoplasmic reticulum stress, and by suppressing nuclear factor-κB activity [26]. Further, betaine demonstrates significant anti-inflammatory function, and is conducive for treating diseases such as cancer, obesity, and diabetes [27–30]. Furthermore, the antioxidant function of betaine can improve oxidative stress induced by asthma [31] or lung injury [32] and protect against lung cancer by reducing the effect of tobacco smoke [33]. Consistently, in our study, low betaine levels were positively associated with reduced levels of DLCO%pred and DLCO/VA%pred in the AD&RC groups. A low betaine level may be indicative of its increased utilization in modulation of the metabolism of sulfur-containing amino acid to combat oxidative stress. This effect could enhance the antioxidant capacity of lungs in AD&RC subjects, thereby providing a potential application of betaine for treating AD&RCs patients in the future.

Adenosine, generated by ATP hydrolysis, accumulates during tissue damage and hypoxia, and may contribute to vasodilatation and reducing inflammation [34, 35] However, the acute increase of adenosine provides anti-inflammatory benefits and a tissue-protective effect, whereas its chronic or long-lasting elevation presents an inverse effect [35]. This phenomenon has also been observed in acute or chronic pulmonary injury. In our study, adenosine levels were low among AD&RCs compared with those in HDs or in participants with normal DLCO. Furthermore, the adenosine level was positively associated with DLCO%pred and DLCO/VA%pred values in AD&RCs. Increasing evidence indicates that adenosine protects cells, including lymphocytes, neutrophils, and macrophages, from

airway inflammation. Therefore, adenosine is a useful biomarker for monitoring airway inflammation, efficacy of anti-inflammatory treatments, and may even aid in COPD and asthma diagnosis [36–39]. Decreased adenosine may be related to airway inflammation in COVID-19 survivors with abnormal DLCO.

Following abnormal DLCO, restrictive ventilatory defects are a major cause of lung function impairment. In our study, levels of methylated and acetylated amino acids, such as methylhistidine, acetylleucine, acetyltyrosine, and acetyl-beta-alanine, were increased in subjects with abnormal TLC readings, compared with those in the normal TLC participants or HDs. Acetyl-amino acids are commonly generated from the hydrolysis of acetylated proteins, and are further catabolized to free amino acids by aminoacylase (ACY) [40]. Further, increased levels of urinary acetyl-amino acids have been found in children with ACY1 deficiency [41]. Methylation and acetylation of DNA and proteins play an important role in many biological processes [42]. Decreased histone acetylation is related to pulmonary fibrosis, whereas the inhibition of histone deacetylase promotes fibroblast apoptosis, both of which provide novel pulmonary fibrosis therapy strategies [43, 44]. Further, increments in levels of methyl- and acetyl-amino acids were negatively correlated with TLC%pred, FVC%pred, and RV%pred levels, suggesting DNA or protein disturbance in abnormal TLC groups.

This study had several limitations. First, this was a single-center prospective study with a relatively small sample size. Second, patients with asymptomatic infection were not included in this study. Third, blood routine tests, liver and kidney function tests, and chest CT findings were not sensitive indicators of the organ injury presented by metabolomics.

Therefore, future large-sized cohort studies using more sensitive measures are warranted.

In conclusion, our results demonstrated that plasma metabolite profiles of COVID-19 survivors with abnormal pulmonary function remarkably differed from those of HDs. Pathway analysis revealed that these alterations related to abnormal pulmonary function mainly involved the metabolic pathways of lysine degradation, and metabolism of taurine, hypotaurine, alpha-linolenic acid, glycerophospholipid, arginine, and proline, as well as arginine biosynthesis.

Supplementary Data

Supplementary materials are available at *Clinical Infectious Diseases* online. Consisting of data provided by the authors to benefit the reader, the posted materials are not copyedited and are the sole responsibility of the authors, so questions or comments should be addressed to the corresponding author.

Nonstandard abbreviations. COVID-19, coronavirus disease-2019; CT, computed tomography; SARS, severe acute respiratory syndrome; RM, mild/moderate patients; RC, severe/critical patients; HD, healthy donors; BMI, body mass index; RP, recovered patients; LC-EST-MS/MS, liquid chromatography-electrospray ionization tandem mass spectrometry; MRM, multiple reaction monitoring; OPLS-DA, orthogonal partial least squares-discriminate analysis; K-W, Kruskal-Wallis test; FDR, false discovery rate; PFTs, pulmonary function tests; TBIL, total bilirubin; DBIL, direct bilirubin; A/G, albumin/globulin; AI, artificial intelligence; GGO, ground-glass opacities; ALP, alkaline phosphatase; ALT, alanine aminotransferase; APTT, activated partial thromboplastin time; AST, aspartate amino transferase; BUN, blood urea nitrogen; CRP, C-reactive protein; Cys-C, cystain C; FIB, fibrinogen; GGT, γ-glutamyl transpeptidase; IQR, interquartile range; LDH, lactate dehydrogenase; PLT, platelet; PT, prothrombin time; TP, total protein; TT, thrombin time; WBCs, white blood cells; TLC, total lung capacity; FRC, functional residual capacity; DLCO, diffusing capacity of the lungs for CO; ND, normal DLCO; AD, abnormal DLCO; ND&RM, recovered mild/moderate patients with normal DLCO%pred; ND&RC, recovered severe/critical patients with normal DLCO%pred; AD&RM, recovered mild/moderate patients with abnormal DLCO%pred; AD&RC, recovered severe/critical patients with abnormal DLCO%pred; CaNO, exhaled alveolar fraction of nitric oxide; FeNO, fractional exhaled nitric oxide; FEV, forced expiratory volume in 1 second; FVC, forced vital capacity; VA, alveolar ventilation; PC, phosphatidylcholines; AC, acetylcarnitine; OA, organic acid; SM, sphingomyelin; AA, amino acid; FA, fatty acid; TG, triacylglycerol; AT, abnormal TLC; NT, normal TLC; ACT, abnormal CT; NCT, normal CT; PGE2, prostaglandin E2; PGE3, prostaglandin E3; IAV, influenza A virus; COPD, chronic obstructive pulmonary disease; ACY, aminoacylase.

Notes

Potential conflicts of interest. The authors: No reported conflicts of interest. All authors have submitted the ICMJE Form for Disclosure of Potential Conflicts of Interest. Conflicts that the editors consider relevant to the content of the manuscript have been disclosed.

References

1. Hui DS, Joynt GM, Wong KT. Impact of severe acute respiratory syndrome (SARS) on pulmonary function, functional capacity and quality of life in a cohort of survivors. Thorax **2015**; 60:401–9.
2. Antonio GE, Wong KT, Hui DS, et al. Thin-section CT in patients with severe acute respiratory syndrome following hospital discharge: preliminary experience. Radiology **2003**; 228:810–5.
3. You J, Zhang L, Ni-Jia-Ti MY, et al. Anormal pulmonary function and residual CT abnormalities in rehabilitating COVID-19 patients after discharge. J Infect **2020**; 81:e150–2.
4. Yu M, Liu Y, Xu D, Zhang R, Lan L, Xu H. Prediction of the development of pulmonary fibrosis using serial thin-section CT and clinical features in patients discharged after treatment for COVID-19 pneumonia. Korean J Radiol **2020**; 21:746–55.
5. Wang Y, Dong C, Hu Y, et al. Temporal changes of CT findings in 90 patients with COVID-19 pneumonia: a longitudinal study. Radiology **2020**; 296:E55–64.
6. Mo X, Jian W, Su Z, et al. Abnormal pulmonary function in COVID-19 patients at time of hospital discharge. Eur Respir J **2020**; 55.
7. Forel J-M, Guervilly C, Hraiech S. Type III procollagen is a reliable marker of ARDS-associated lung fibroproliferation. Intensive Care Med **2015**; 41:1–11.
8. Gupta A, Madhavan MV, Sehgal K, et al. Extrapulmonary manifestations of COVID-19. Nat Med **2020**; 26:1017–32.
9. Shi H, Han X, Jiang N, et al. Radiological findings from 81 patients with COVID-19 pneumonia in Wuhan, China: a descriptive study. Lancet Infect Dis **2020**; 20:425–34.
10. Hu S, Hoffman EA, Reinhardt JM. Automatic lung segmentation for accurate quantitation of volumetric X-ray CT images. IEEE Trans Med Imaging **2001**; 20:490–8.
11. Graham BL, Steenbruggen I, Miller MR, et al. Standardization of spirometry 2019 update. An official American Thoracic Society and European Respiratory Society technical statement. Am J Respir Crit Care Med **2019**; 200:e70–88.
12. Wu D, Shu T, Yang X, et al. Plasma metabolomic and lipidomic alterations associated with COVID-19. Natl Sci Rev **2020**; 7:1157–68.
13. Song JW, Lam SM, Fan X, et al. Omics-driven systems interrogation of metabolic dysregulation in COVID-19 pathogenesis. Cell metabolism **2020**; 32:188–202 e185.
14. Shen B, Yi X, Sun Y, et al. Proteomic and metabolomic characterization of COVID-19 patient sera. Cell **2020**; 182:59–72 e15.
15. Sui X, Wang K, Gluchowski NL, et al. Structure and catalytic mechanism of a human triacylglycerol-synthesis enzyme. Nature **2020**; 581:323–8.
16. Enzi G, Bevilacqua M, Crepaldi G. Disturbances in pulmonary gaseous exchange in primary hyperlipoproteinemias. Bull Eur Physiopathol Respir **1976**; 12:433–42.
17. Park JY, Pillinger MH, Abramson SB. Prostaglandin E2 synthesis and secretion: the role of PGE2 synthases. Clinical immunology **2006**; 119:229–40.
18. Coulombe F, Jaworska J, Verway M, et al. Targeted prostaglandin E2 inhibition enhances antiviral immunity through induction of type I interferon and apoptosis in macrophages. Immunity **2014**; 40:554–68.
19. Toller IM, Hitzler I, Sayi A, Mueller A. Prostaglandin E2 prevents Helicobacter-induced gastric preneoplasia and facilitates persistent infection in a mouse model. Gastroenterology **2010**; 138:1455–67.
20. Horikiri T, Hara H, Saito N, et al. Increased levels of prostaglandin E-major urinary metabolite (PGE-MUM) in chronic fibrosing interstitial pneumonia. Respir Med **2017**; 122:43–50.
21. Uzan GC, Borekci S, Doventas YE, Koldas MBG. The relationship between inflammatory markers and spirometric parameters in ACOS, asthma, and COPD. J Asthma **2019**; 12: 1–7.
22. Geiger R, Rieckmann JC, Wolf T. L-arginine modulates T cell metabolism and enhances survival and anti-tumor activity. Cell **2016**; 167: 829–42.

23. Mehl A, Ghorbani P, Douda D, et al. Effect of arginase inhibition on pulmonary L-arginine metabolism in murine Pseudomonas pneumonia. PLoS One **2014**; 9:e90232.

24. Pera T, Zuidhof AB, Smit M, et al. Arginase inhibition prevents inflammation and remodeling in a guinea pig model of chronic obstructive pulmonary disease. J Pharmacol Exp Ther **2014**; 349:229–38.

25. Moncada S, Higgs A. The L-arginine-nitric oxide pathway. N Engl J Med **1993**; 329: 2002–12.

26. Zhao G, He F, Wu C, et al. Betaine in inflammation: mechanistic aspects and applications. Front Immunol **2018**; 9:1070.

27. Chen YM, Liu Y, Liu YH, Wang X, Guan K, Zhu HL. Higher serum concentrations of betaine rather than choline is associated with better profiles of DXA-derived body fat and fat distribution in Chinese adults. Int J Obes (Lond) **2015**; 39:465–71.

28. Gao X, Randell E, Zhou H, Sun G. Higher serum choline and betaine levels are associated with better body composition in male but not female population. PLoS One **2018**; 13:e0193114.

29. Chen L, Chen YM, Wang LJ, et al. Higher homocysteine and lower betaine increase the risk of microangiopathy in patients with diabetes mellitus carrying the GG genotype of PEMT G774C. Diabetes Metab Res Rev **2013**; 29:607–17.

30. Detopoulou P, Panagiotakos DB, Antonopoulou S, Pitsavos C, Stefanadis C. Dietary choline and betaine intakes in relation to concentrations of inflammatory markers in healthy adults: the ATTICA study. Am J Clin Nutr **2008**; 87:424–30.

31. Pourmehdi A, Sakhaei Z, Alirezaei M, Dezfoulian O. Betaine effects against asthma-induced oxidative stress in the liver and kidney of mice. Mol Biol Rep **2020**; 47:5729–35.

32. Na JD, Choi YJ, Jun DS, Kim YC. Alleviation of paraquat-induced oxidative lung injury by betaine via regulation of sulfur-containing amino acid metabolism despite the lack of betaine-homocysteine methyltransferase (BHMT) in the lung. Food Funct **2019**; 10:1225–34.

33. Ying J, Rahbar MH, Hallman DM, et al. Associations between dietary intake of choline and betaine and lung cancer risk. PLoS One **2013**; 8:e54561.

34. Haskó G, Antonioli L, Cronstein BN. Adenosine metabolism, immunity and joint health. Biochem Pharmacol **2018**; 151: 307–313.

35. Borea PA, Gessi S, Merighi S, Vincenzi F, Varani K. Pathological overproduction: the bad side of adenosine. Br J Pharmacol **2017**; 174:1945–60.

36. Cushley MJ, Tattersfield AE, Holgate ST. Inhaled adenosine and guanosine on airway resistance in normal and asthmatic subjects. Br J Clin Pharmacol **1983**; 15:161–5.

37. Newby AC. Adenosine and the concept of retaliatory metabolites. Trends Biochem Sci **1984**; 9: 42–44.

38. Mubagwa K, Mullane K, Flameng W. Role of adenosine in the heart and circulation. Cardiovasc Res **1996**; 32:797–813.

39. Spicuzza L, Di Maria G, Polosa R. Adenosine in the airways: implications and applications. Eur J Pharmacol **2006**; 533:77–88.

40. Jones WM, Scaloni A, Bossa F, Popowicz AM, Schneewind O, Manning JM. Genetic relationship between acylpeptide hydrolase and acylase, two hydrolytic enzymes with similar binding but different catalytic specificities. Proc Natl Acad Sci U S A **1991**; 88:2194–8.

41. Baltimore M. Online Mendelian Inheritance in Man OMIM (TM). Johns Hopkins University. http://www.ncbi.nlm.nih.gov/omim. Accessed 20 October 2020.

42. Su X, Wellen KE, Rabinowitz JD. Metabolic control of methylation and acetylation. Curr Opin Chem Biol **2016**; 30:52–60.

43. Sanders YY, Hagood JS, Liu H, Zhang W, Ambalavanan N, Thannickal VJ. Histone deacetylase inhibition promotes fibroblast apoptosis and ameliorates pulmonary fibrosis in mice. Eur Respir J **2014**; 43:1448–58.

44. Huang SK, Scruggs AM, Donaghy J, et al. Histone modifications are responsible for decreased Fas expression and apoptosis resistance in fibrotic lung fibroblasts. Cell Death Dis **2013**; 4:e621.